SPH MODELLING FOR 3D URBAN DAM-BREAK FLOODS, WITH DAMAGE ASSESSMENT TO ELECTRICAL SUBSTATIONS

Andrea Amicarelli[1,0], Sauro Manenti[2], Marco Paggi[3]
[1]Ricerca sul Sistema Energetico - RSE SpA, Department SFE, via Rubattino, 54, 20134, Milan, Italy
[2]Dipartimento di Ingegneria Civile e Architettura (DICAr), via Ferrata 3, 27100 Pavia, Italy
[3]IMT School for Advanced Studies Lucca, Piazza San Francesco 19, 55100 Lucca, Italy

[0]Corresponding author
andrea.amicarelli@rse-web.it sauro.manenti@unipv.it marco.paggi@imtlucca.it

Abstract
The Smoothed Particle Hydrodynamics code SPHERA (RSE SpA) is validated on a laboratory urban dam-break flood. Comparisons with a porous Shallow Water Equations - Finite Volume Method 2D model are also reported. SPHERA provides a performance comparable with the state-of-the-art code, with results closer to the measured values during the most risky flood stage. Some improvements of SPHERA predictions are achieved by a direct modelling of the mobile gate triggering the flood. SPHERA is also empowered with a substation-flooding damage model, which distinguishes the functional damage due to the substation out of service from the material damage to the substation components. SPHERA is finally applied to a full-scale catastrophic 3D dam-break flood, which interacts with a lower hydroelectric reservoir, covers four residential areas and two electrical substations, whose related damage is assessed. SPHERA is distributed on a GitHub public repository, included the input files of this study.

Keywords
SPH; urban floods; dam breaks; substation-flooding damage model; electrical substations.

1. INTRODUCTION

Floods represent a major category of natural disasters in terms of both number of fatalities and economic damage (Munich RE, 2010, [42]) and, compared to such categories, affect the highest number of people (EM-DAT, 2012, [16]).

Among the targets of the electric system, floods impact electrical stations and substations, power lines and energy storage plants. The direct and indirect damage are related to: blackouts and brownouts; structures, electricity pylons and electrical substations; functional damage and alteration in the protection level of the electrical components/machines/devices, among the others.

Hydroelectric plants play a triple role: they can trigger a flood (overtopping, breaks, structural failures of dams/gates), be a flood target (Technological accidents triggered by Natural disasters - NaTech accidents -) or represent overflow dams (flood-control works).

The main causes of power outages (blackout events) are classified as follows: excessive electric power request; failures on electric stations (e.g., out of order status), substations (e.g., flooding) and power transmission and distribution lines (e.g., due to accidents or intense natural events); sabotage acts; loss of international connections.

Floods are classified among the main categories of meteorological and hydrogeological risky events for the electrical grids, listed hereafter: floods, intense rain and soil saturation; snow and ice; temperature increase, heath waves and droughts; coastal flood erosion; fluvial erosion; storms, gusts and strong wind (Electricity North West Limited, 2017, [15]).

As an example, Electricity North West Limited (2017, [15]) considers floods as the most severe climatic risk for the power grids in the United Kingdom, both at present and future (as resulting from the increase in precipitation and sea level). As a matter of fact, flooding of electrical substations is one of the main failure modes of the power grid together with wind-induced damage on the transmission power lines (Holmes, 2015, [26]). The associated and severe climatic risk can be quantified by approximately increasing of 20% the expected water depth in absence of climate changes (Electricity North West Limited, 2017, [15]; Holmes, 2015, [26]).

The expression “electrical substations” here refers to the ensemble of the following categories, associated with different economic values: high-voltage transmission electrical substations; medium-voltage distribution electrical substations; low-voltage distribution electrical substations. The low-voltage substations mounted on poles are not considered by this study as they refer to the risk on distribution power lines (Holmes, 2015, [26]). Hereafter are listed the flood-control structural actions implemented by the National Grid within the areas of the electrical substations (Electricity North West Limited, 2017, [15]): gates; earth-filled dikes; rising of foundations and electric components; addition of floating devices and stilts; increase in the power grid interconnection (redundancy); local sandscaping for coastlines and water body banks; mobile barrier systems (to mitigate the short-term risk).

Few 2D Computational Fluid Dynamics (CFD) - Finite Volume Method (FVM) codes, based on the Shallow Water Equations (SWE), have been validated on urban floods (e.g., Yu et al., 2005, [59]; Sanders, 2008, [45]; Chen et al., 2012, [9]; Schubert & Sanders, 2012, [47]). More recently, a CFD-FVM-SWE variant is represented by SWE porous models, which allow not to explicitly solve the fluid dynamics fields within the urban canopy (ensemble of the urban streets and buildings), but using a coarser spatial resolution and fractioning the contributions of the balance equation terms based on the porosity of the mesh cells. Herein porosity is defined as the cell volume fraction filled with liquid (e.g., Cea & Vázquez-Cendón, 2010; Soares-Frazão et al., 2008, [51]; Sanders et al., 2008, [46]; Guinot, 2012, [21]; Kim et al., 2015, [30]).

Among the few numerical tools focused on urban floods, Smoothed Particle Hydrodynamics (SPH) modelling represents a valuable numerical method of Computational Fluid Dynamics (CFD) particularly suitable for the simulation of 3D floods, hydraulic works of hydroelectric plants, fast landslides and wave motion, sediment removal from water reservoirs. Hereafter a brief introduction to SPH is reported.

SPH computational nodes are represented by numerical fluid particles. In the continuum, the functions and derivatives in the fluid dynamics balance equations are approximated by convolution integrals, which are weighted by interpolating (or smoothing functions), called kernel functions.
The integral SPH approximation ($<>_I$) of a generic function (f) is defined as:

$$\left\langle f \right\rangle_{I,\underline{x}_0} = \int_{V_h} f W dx^3 \tag{1.1}$$

where W (m^{-3}) is the kernel function (Monaghan, 2005, [41]), $\underline{x}_0$ (m) is the position of a generic computational point and V_h (m^3) is the integration volume, which is called kernel support. This is represented by a sphere of radius $2h$ (m), possibly truncated by the frontiers of the fluid domain.
Any first derivative of a generic function, calculated along i-axis, can be computed as in (1.1), after replacing f with the targeted derivative. After integration by parts, one obtains:

$$\left\langle \frac{\partial f}{\partial x_i} \right\rangle_{I,\underline{x}_0} = \int_{A_h} f W n_i dx^2 - \int_{V_h} f \frac{\partial W}{\partial x_i} dx^3 \tag{1.2}$$

The integration also involves the surface A_h (m^2) of the kernel support. The associated surface integral is non-zero in case of a truncated kernel support. The representation of this term noticeably differentiates the various SPH codes developed by the research community (Adami et al., 2012, [2]; Hashemi et al., 2012, [23]; Macia et al., 2012, [33]; Mayrhofer et al., 2013, [39]; Ferrand et al., 2013, [18]; Amicarelli et al., 2013, [3]).
Far from boundaries, the SPH particle approximation of (1.2) reads:

$$\left\langle \frac{\partial f}{\partial x_i} \right\rangle_{\underline{x}_0} = -\sum_b f_b \left. \frac{\partial W}{\partial x_i} \right|_b \omega_b \tag{1.3}$$

where a summation on particle volumes ω (m^3) replaces the volume integral. The subscripts "$_0$" and "$_b$" refer to the computational particle and its "neighbouring particles" (fluid particles within the kernel support of the computational particle), respectively.
Usually, the approximation (1.3) is replaced by more complicated and accurate formulae. Further, the SPH method can also approximate a generic n-th derivative, analogously to (1.3).
Among the various numerical methods, Smoothed Particle Hydrodynamics (SPH) has several advantages: a direct estimation of free surface and phase/fluid interfaces; effective simulations of multiple moving bodies and particulate matter within fluid flows; direct estimation of Lagrangian derivatives (absence of non-linear advective terms in the balance equations); effective numerical simulation of fast transient phenomena; no meshing; simple non-iterative algorithms (in case the "Weakly Compressible" approach is adopted). On the other hand, SPH models are affected by the following drawbacks, if compared with mesh-based CFD tools: computational costs are slightly higher due to a larger stencil (around each computational particle), which causes a high number of interacting elements (neighbouring particles) at a fixed time step (nonetheless SPH codes are more suitable to parallelization); local refining of spatial resolution represents a current issue and is only addressed by few advanced and complex SPH algorithms; accuracy is relatively low for classical CFD applications where mesh-based methods are well established (e.g., confined mono-phase flows). Detailed reviews on SPH assets and drawbacks have been reported in Gomez-Gesteira et al. (2010, [19]), Le Touzé et al. (2013, [31]), Shadloo et al. (2016, [48]),Violeau & Rogers (2016, [57]). Nevertheless, SPH models are effective in many, but peculiar, application fields. Some of them are herein briefly recalled: free-surface flows (e.g., Tsuruta et al., 2015, [53]); sloshing tanks (e.g., Amicarelli et al., 2013, [3]); gravitational surface waves (e.g. Colagrossi et al., 2013, [11]); hydraulic turbines (e.g., Marongiu et al., 2010, [38]); liquid jets (e.g., Marongiu et al., 2010, [38]); astrophysics and magneto-hydrodynamics (e.g., Price, 2012, [43]); body dynamics in free surface flows (e.g., Amicarelli et al., 2015, [4]); fluid - flexible structure interactions (e.g., Khayyer et al., 2018, [29]); multi-phase and multi-fluid flows (e.g., Wan et al., 2017, [58]; He et al., 2017, [25]); sediment removal from water reservoirs (e.g., Manenti et al., 2012, [37]); landslides (e.g.,

Abdelrazek et al., 2016, [1]; Bui et al., 2008, [7]); natural convection (e.g., Danis et al., 2012, [13]). The SPH numerical method has also been successfully applied to flood propagation, as synthesized in the following. Vacondio et al. (2012, [54]) presents the Shallow-Water-Equation (SWE) variant of the SPH code SPHysics (Johns Hopkins University et al.) for flooding. Inlet/outlet treatment is dealt with 1D Riemann invariants. Several 1D validations refer to analytical solutions (e.g., flows over a bump). The code is validated on the 3D Okushiri tsunami scaled test case. Gu et al. (2017, [20]) analogously apply the same code to represent scaled dam breaks with obstacles for validating purposes. They also provide a full scale demonstration with a possible dam break scenario for the South-Gate Gorges Reservoir (China). Liang et al. (2015, [32]) presents a SPH-SWE code for GPU cards for efficient urban flood modelling providing demonstrations on full-scale urban floods. Guo et al. (2017, [22]) validate a SPH model on the flooding of a rigid floating structure with 6 degrees of freedom. Manenti et al. (2019, [36]) report a review on the SPH models for water-related natural hazards focusing on the following topics: rapidly varied flows of water or dense granular flows; sediment erosion; bed-load transport; flooding on complex topography; fast landslides and induced surge waves; High Performance Computing techniques.

The present study takes benefit from the SPH method features to simulate urban floods, introducing the following peculiar features: 3D (non-SWE) SPH modelling on floods propagating over real full-scale topography; catastrophic dam-break scenario on real topography; 3D validation on a scaled urban dam-break flood with explicit representation of buildings; simultaneous modelling of 3D solid bodies and transported sediments; damage model for the flooding of electrical substations. The SPH FOSS (Free/Libre and Open-Source Software) code SPHERA v.9.0.0 (2019, RSE SpA, [49]) is validated on the experimental dataset reported in Kim et al. (2015, [30]), which represents two scenarios of an urban dam-break flood. A water reservoir is interested by a dam break event triggered by the fast and regular opening of a mobile gate. The following flood covers a stylised urban environment represented by 2 matrices of buildings (18 structures in all) and the associated urban canyons, located over a floodplain. Inter-comparisons and advantages with respect to the state-of-the-art code are also analysed. Further, a substation-flooding damage model is formulated and implemented in SPHERA. The model distinguishes damage due to the substation out of service from damage to the components of the electrical substations. SPHERA is applied to a 3D demonstrative test case, the Alpe Gera dam-break flood (Italy), which interacts with the lower hydroelectric reservoir of Campo Moro and propagates over the residential areas of Lanzada's municipality (Lanzada, Franscia, Tornadri e Ganda; province of Sondrio, Italy), causing the flooding of two electrical substations of Lanzada (with assessment of the associated damage). Some innovative features are highlighted: the representation of a dam-break flood by means of a 3D SPH-CFD code on complex topography, as a possible catastrophe triggered by an accident in a major power plant; the 3D CFD-SPH simulation of a flood propagating over several residential areas; the application of the substation-flooding damage model on a real and complex test case, with the simultaneous representation of several electrical substations.

The paper is organized as follows: the features of the code SPHERA are synthesized (Sec.2); the substation-flooding damage scheme is presented (Sec.3); the results of the code validation on the experimental urban dam-break flood are shown (Sec.4); the application to a 3D dam-break flood with real full-scale topography, residential areas and electrical substations is discussed (Sec.5); the overall conclusions are summarized (Sec.6).

2. THE NUMERICAL MODEL

SPHERA v.9.0.0 (RSE SpA, 2019, [49]) is research FOSS ("Free/Libre and Open-Source Software") based on the SPH method. SPHERA has been applied to floods (with transport of solid bodies, bed-load transport and a domain spatial coverage up to some hundreds of squared kilometres), fast landslides and wave motion, sediment removal from water reservoirs, sloshing tanks, hydrodynamic lubrication.

The main numerical developments featuring SPHERA v.9.0.0 are listed hereafter: a scheme for dense granular flows (Amicarelli et al., 2017, [5]); a scheme for the transport of solid bodies in free surface flows (Amicarelli et al., 2015, [4]); a scheme for a boundary treatment ("DB-SPH" for simplicity of notation) based on discrete surface and volume elements, and on a 1D Linearized Partial Riemann Solver coupled with a MUSCL (Monotonic Upstream-Centered Scheme for Conservation Laws) spatial reconstruction scheme (Amicarelli et al., 2013, [3]); a scheme for a 2D erosion criterion (Manenti et al., 2012, [37]); a scheme for a boundary treatment ("semi-analytic approach or SA-SPH" for simplicity of notation) based on volume integrals, numerically computed outside of the fluid domain (Di Monaco et al., 2011, [14]).

SPHERA shares the same drawbacks featuring the SPH state-of-the-art, with respect to analogous mesh-based CFD models: SPHERA is not a general-purpose CFD code, has no multi-resolution approach and the high number of neighbouring particles might penalise the computational time, despite the high suitability of SPH models to parallelization and their simple algorithms. Further, although SPHERA makes use of several High Performance Computing solutions (OMP parallelization, pre-processor directives, optimization compilation options), they could be improved and the code could be also parallelized by means of the MPI technique.

Some of the features of SPHERA used for this study are synthesized in the following.

The numerical scheme for the main flow is a Weakly-Compressible (WC) SPH model, which takes benefit from a boundary treatment for fixed boundaries based on the semi-analytic approach of Vila (1999, [55]), as developed by Di Monaco et al. (2011, [14]).

One considers Euler's momentum and continuity equations:

$$\begin{aligned} \frac{du_i}{dt} &= -\frac{1}{\rho}\frac{\partial p}{\partial x_i} - \delta_{i3} g, \qquad i = 1,2,3 \\ \frac{d\rho}{dt} &= -\rho \nabla \cdot \underline{u} \end{aligned} \tag{2.1}$$

where $\underline{u} \equiv (u,v,w)$ (m/s) is the velocity vector, p (Pa) is the pressure, ρ (kg/m^3) is the fluid density, δ_{ij} is Kronecker's delta function and t (s) denotes time. One needs to compute (2.1) at each fluid particle position by using the SPH formalism and by taking into account the boundary terms (fluid-frontier and fluid-body interactions), as described below.

One considers the discretization of (2.1), as provided by the SPH approximation of the first derivative of a generic function (f), according to the semi-analytic approach ("SA"; Vila, 1999, [55]):

$$\left\langle \frac{\partial f}{\partial x_i} \right\rangle_{SA,0} = -\sum_b (f_b - f_0)\frac{\partial W_b}{\partial x_i}\omega_b - \int_{V_h'} (f - f_0)\frac{\partial W}{\partial x_i} dx^3 \tag{2.2}$$

The inner fluid domain here involved is filled with numerical particles. At boundaries, the kernel support is formally not truncated because it can partially lie outside the fluid domain. In other words, the summation in (2.2) is performed over all the fluid particles "$_b$" (neighbouring particles with volume ω) in the kernel support of the computational fluid particle ("$_0$"). At the same time, the volume integral in (2.2) represents the boundary term, which is a convolution integral on the truncated portion of the kernel support. In this fictitious and outer volume V_h' (m^3), one needs to define the generic function f (pressure, velocity or density alternatively), as in Di Monaco et al. (2011, [14]).

The continuity equation for a Weakly Compressible SPH model assumes the following form, where Einstein's notation is herein adopted for the subscript "$_j$" and the semi-analytic approach (Di Monaco et al., 2011) expresses the boundary integral term at the fixed frontiers (second term on the Right Hand Side):

$$\left\langle \frac{d\rho}{dt} \right\rangle_0 = \sum_b \rho_b \left(u_{b,j} - u_{0,j}\right) \left. \frac{\partial W}{\partial x_j} \right|_b \omega_b + 2\rho_0 \int_{V_h'} \left[\left(\underline{u}_w - \underline{u}_0\right) \cdot \underline{n} \right] n_j \frac{\partial W}{\partial x_j} dx^3 + C_s \tag{2.3}$$

C_s (kg×m^{-3}×s^{-1}) is introduced to represent the fluid-body interaction term (Amicarelli et al., 2015, [4]; Amicarelli et al., 2020, [6]).

The SPH approximation ($\langle\ \rangle$) of the momentum equationreads (Amicarelli et al., 2020, [6])::

$$\left\langle \frac{du_i}{dt} \right\rangle_0 = -\delta_{i3} g + \sum_b \left(\frac{p_b}{\rho_b^2} + \frac{p_0}{\rho_0^2} \right) \left. \frac{\partial W}{\partial x_i} \right|_b m_b +$$

$$+ 2\frac{p_0}{\rho_0} \int_{V_h'} \frac{\partial W}{\partial x_i} dx^3 - \upsilon_M \sum_b \frac{m_b}{\rho_0 r_{0b}^2} \left(\underline{u}_b - \underline{u}_0\right) \cdot \left(\underline{x}_b - \underline{x}_0\right) \left. \frac{\partial W}{\partial x_i} \right|_b + \tag{2.4}$$

$$- 2\upsilon_M \left(\underline{u}_w - \underline{u}_0\right) \cdot \int_{V_h'} \frac{1}{r_{0w}^2} \left(\underline{x} - \underline{x}_0\right) \left. \frac{\partial W}{\partial x_i} \right|_b dx^3 + \underline{a}_s + 2\nu_0 \left(\underline{u}_w - \underline{u}_0\right) \int_{V_h'} \frac{1}{r} \left| \frac{\partial W}{\partial r} \right|_b dx^3$$

where $\underline{a}_s$ (m×s^{-2}) represents a new acceleration term due to the fluid-body interactions (Amicarelli et al., 2015, [4]; Amicarelli et al., 2020, [6]), ν_M (m^2×s^{-1}) is the artificial viscosity (Monaghan, 2005, [41]), m (kg) is the particle mass and r (m) is the relative distance between the neighbouring and the computational particle.

Finally, a barotropic equation of state (EOS) is linearized as follows:

$$p \cong c_{ref}^2 \left(\rho - \rho_{ref}\right) \tag{2.5}$$

The artificial sound speed c (m/s) is 10 times higher than the maximum fluid velocity (WC approach) and "$_{ref}$" stands for a reference state.

More details are available in Amicarelli et al. (2015, [4]), Di Monaco et al. (2011, [14]) and Amicarelli et al. (2020, [6]).

Time integration is ruled by a second-order Leapfrog scheme, as described in Di Monaco et al. (2011, [14]) and Amicarelli et al. (2015, [4]). Stability analysis and time integration schemes in SPH modelling are discussed in Violeau and Leroy (2014, [56]),

3. SUBSTATION-FLOODING DAMAGE SCHEME

A damage scheme for the flooding of electrical substations is presented and integrated in SPHERA (2019, [49]). The model distinguishes the functional damage due to the substation out of service from the material damage to the components of the electrical substations. Considering the out of service, a formulation of "proxy" damage (in time units) is presented. The substation out of service might cause a blackout event. In the following, one assumes (as a simplifying hypothesis) no redundancy of the local power grid, so that the failure of an electrical substation triggers a blackout event in a grid branch (no matter about its length and connections). This assumption only allows using indifferently the expression "power outage" ("blackout event") or "substation out of service". The assessment of the overall vulnerability of the electric grid and the global damage (in monetary units) due to flood-related blackout events is out of the aims of this study and would need: the coupling of the present model with a power grid model; the maps of the exposed population, the values of the public (also environmental) and private goods, the activities affected by the blackout and their flood-related vulnerability curves. On the other hand, considering the components of the electrical substations, a complete model is presented for direct and tangible damage.

The substation-flooding damage model estimates the following physical quantities, at every electrical substation: the Probability of a power Outage Start (*POS*) as function of the maximum substation water depth; the Expected power Outage Status (*EOS*), at the level of the single electrical substations (in the absence of power grid redundancy); Expected Outage Time/duration (*EOT*, s); the flood-related vulnerability and damage (euros) limited to the components of the electrical substations.

3.1. Mathematical models

3.1.1. Flood-induced functional damage due to the substation out of service

A proxy damage formulation quantifies in time units the damage due to the out of service of electrical substations flooded. One assumes that the malfunction of a substation determines a blackout event in a branch of the power grid (simplifying hypothesis of no redundancy).

The breakdown in the electrical energy supply is analysed only considering the power outage events and neglecting the damage due to brownouts (voltage drops).

The Probability of an Outage Start (*POS*) (i.e. the probability of triggering a blackout event) at a fixed time is smaller than (or equal to) the probability of occurrence of a blackout event at the same time (*EOS*, "Expected Outage Status") because the latter also depends on the blackout events which might start previously.

The procedure of HAZUS-MH (2011, [24]) considers a threshold water depth of Y_{th}=1.2m for blackout events associated with the flooding of electrical substation. However, the above procedure does not mention either data or the method to elaborate them. Holmes (2015, [26]) explains that the above threshold value is overestimated. In particular, the majority of the UK electrical substations has shown a threshold of Y_{th}=0.30m (Crawford & Seidel, 2013, [12]). Considering this value and a maximum threshold of $Y_{th,max}$=0.50m, Holmes (2015, [26]) provides a linear relationship between the probability of an Outage Start and water depth, here assumed as spatial average over the territory belonging to the electrical substation (Y_{sub}, m):

$$POS\big|_{t=t^*} = \begin{cases} 1, & Y_{sub}\big|_{t=t^*} \geq 0.52 \\ 1.92Y, & 0 < Y_{sub}\big|_{t=t^*} < 0.52 \\ 0, & Y_{sub}\big|_{t=t^*} = 0 \end{cases} \tag{3.1}$$

The above relationship has been validated on other open-field data (Holmes, 2015, [26]).

The "Expected Outage Status" is defined as a binary variable which represents either the expected presence (*EOS*=1) or the expected absence (*EOS*=0) of a blackout event at a fixed time, at the level of the single electrical substation:

$$EOS\big|_{t=t^*} = \begin{cases} 1, & \sum_i \max\left\{\left(POS\big|_{t=t_i} - 0.49\right), 0\right\} > 0, \quad t^* - t_{rei,e} \le t_i \le t^* \\ 0, & otherwise \end{cases} \tag{3.2}$$

EOS is unity if at least once, during the period before the on-going time ($t=t^*$) lasting the restoration time of the electrical infrastructures ($t_{rei,e}$), *POS* is greater than 0.5.

The values of $t_{rei,e}$ are commonly greater for smaller substations with less redundancy. This time scale has been quantified by several authors: Chow et al. (1996, [10]) report the interval t_{rei}=0'-500'; Maliszewski & Perrings (2012, [34]) suggest an average value of $t_{rei,e}$=99' and a maximum value of $t_{rei,max}$=330'. Both the above references consider a typical value of t_{rei} smaller than two hours. However, their analyses only consider blackout events under normal (non-extreme) environmental conditions. Reed (2008, [44]) proposes to use a particular realization of the "gamma" probability density function, for t_{rei} on blackouts induced by intense meteorological and flood events.

Considering a null minimum value and a maximum value (under the worst hypothesis) of 22 hours (95th percentile of the "gamma" distribution of Reed -2008, [44]-), the present model assumes an expected restoration time of 11 hours ($t_{rei,e}$=39'600s), in the absence of further data and in favour of safety.

The system (3.1)-(3.2) represents a formulation of the vulnerability of the single electrical substation to the flood-induced blackout events, in the absence of redundancy.

The "Expected Outage Time" (*EOT*, s) is here defined as the expected cumulated duration of the sub-periods of blackout:

$$EOT\big|_{t=t^*} = \sum_i EOS_{t=t_i} \Delta t\big|_{t=t_i}, \qquad t_0 \le t_i \le t_f \tag{3.3}$$

where Δt is the model time step duration. The subscripts "$_0$", "$_f$" and "$_i$" represent initial conditions, final conditions and a generic time step, respectively. A blackout event can involve several interruptions and the following relationship is assumed: $EOT \ge t_{rei,e}$. Eq.(3.3) represents a formulation of the "proxy" damage (quantified in time units) due to flood-induced blackout events, in the absence of redundancy(at the level of the single substations).

3.1.2. Flood-induced material damage to the components of the electrical substations

This mathematical model assesses the (direct and tangible) damage induced by floods to the components of the electrical substations (D_{sub}). This damage model is complete as it quantifies both vulnerability and damage (the latter in monetary units):

$$D_{sub}\big|_{t=t^*} = V_{u,sub}\big|_{t=t^*} \cdot V_{a,sub} \tag{3.4}$$

The value of the electrical substations ($V_{a,sub}$) can be expressed in US dollars (HAZUS-MH, 2011, [24]):

$$V_{a,sub} = \begin{cases} 50'000, & High-Voltage-Substation \\ 20'000, & Medium-Voltage-Substation \\ 10'000, & Low-Voltage-Substation \end{cases} \tag{3.5}$$

but SPHERA works in euros (currency exchange rate of February 2018):

$$V_{a,sub} = \begin{cases} 41'000, & High-Voltage-Substation \\ 16'400, & Medium-Voltage-Substation \\ 8'200, & Low-Voltage-Substation \end{cases} \tag{3.6}$$

$V_{u,sub}$ is the vulnerability of an electrical substation with respect to the (direct and tangible) flood-induced damage involving the substation components. This model provides a regression curve (6th degree polynomial function) for $V_{u,sub}$, after elaboration of the point values reported by HAZUS-MH (2011, [24]):

$$V_{u.sub}\big|_{t=t^*}=\begin{cases}0.15, & \left(Y_{sub,max}\big|_{t\le t^*}\right)\ge 10\\ \left(a\left(Y_{sub,max}\big|_{t\le t^*}\right)^6+b\left(Y_{sub,max}\big|_{t\le t^*}\right)^5+c\left(Y_{sub,max}\big|_{t\le t^*}\right)^4+\right. & 0<\left(Y_{sub,max}\big|_{t\le t^*}\right)<10\\ \left.+d\left(Y_{sub,max}\big|_{t\le t^*}\right)^3+e\left(Y_{sub,max}\big|_{t\le t^*}\right)^2+f\left(Y_{sub,max}\big|_{t\le t^*}\right)\right), & \\ 0, & \left(Y_{sub,max}\big|_{t\le t^*}\right)=0\end{cases} \quad (3.7)$$

where the maximum value of the substation water depth $Y_{sub,max}$ refers to the period simulated until the on-going time ($t=t^*$). The regression procedure provides the following constants: a=-1.22877·10^{-6}m^{-6}, b=1.92478·10^{-5}m^{-5}, c=8.4216·10^{-6}m^{-4}, d=-0.00119121m^{-3}, e=0.00390726m^{-2}, f=0.0170243m^{-1}.

3.2. Numerical features

The discretization of the mathematical models of Sec.3.1 involves some numerical features herein discussed.

At the beginning of the simulation the following procedures are executed:

- ✓ identification of the DEM vertices internal to the polygons (representing the electrical substations in plan view);
- ✓ assessment of the areas of the above polygons (represented by triangles, quadrilaterals, pentagons and hexagons);
- ✓ initialization of the variables of the electrical substations.

At the end of each output writing time step of the damage model, the following procedures are executed for every electrical substation:

- ✓ assessment of the variable Y_{sub} as spatial average of the water depth values at the DEM vertices within the polygon of the electrical substation;
- ✓ update of the variable $Y_{sub,max}$;
- ✓ assessment of the variables *POS* and *EOS*;
- ✓ update of the variables *EOT*, D_{sub} and $V_{u,sub}$;
- ✓ writing of the output file for the vulnerability and damage variables.

The water depths at the DEM points are saved and stored until the following time step.

With reference to the application of Sec.5, the map of the Italian electrical stations, substations and transmission lines is available at MATTM (2019, [40]). It is useful to activate the layer of OpenStreetMap and the "aerial view" of Bing to detect the electrical stations (squares), substations (polygons) and transmission lines (lines), as well as the electricity pylons (nodes/points). Contrarily, the feature "Atlarete Linee" seems more imprecise (some symbols of the electrical stations would represent electricity pylons; the electrical substations do not seem to represent the nodes of the transmission power grid).

4. VALIDATION: 3D URBAN DAM-BREAK FLOOD

SPHERA is validated on the dataset of Kim et al. (2015, [30]), which represents an experimental urban dam-break flood. A water reservoir (Figure 4.1) is interested by a dam break event triggered by the fast and regular opening of a mobile gate. The following flood covers a stylised urban environment represented by 2 matrices of buildings (18 structures in all) and the associated urban canyons, located over a floodplain.

The coordinates of the barycentres of the 9 buildings in the numerical domain (Figure 4.1) are reported in Table 4.1. Each building has the following dimensions: 0.200m×0.200m×0.500m. The building matrix is anisotropic with spacing along *x*- and *y*- axes equal to $\Delta x_{B,x}$=0.100m and $\Delta x_{B,y}$=0.400m, respectively. This configuration implies the presence of large street canyons perpendicular to narrow street canyons. The building height is not explicitly declared, but it should be sufficiently high to avoid the street canyon overtopping. The SPH simulations assume the building height to be equal to $z_{B,top}$=0.500m.

The experimental dataset defines two scenarios, which only differ on the initial reservoir water depth: $h_{res,0,sc1}$=0.300m ("scenario 1") and $h_{res,0,sc2}$=0.450m ("scenario 2"). In both cases, the phenomenon is clearly exhausted at the final time t_f=600s.

Eleven probes (lines) monitor the hydrographs of the water depth to compare the simulated values with the available measures (validation) and numerical data (inter-comparison). The experimental sampling frequency is dt_{exp}=0.2s. Table 4.2 reports the coordinates of the monitoring lines (i.e. the experimental probes P_i. i>0) and the additional numerical probe P_0 located at the reservoir outlet sections (within the plane y=-0.250 m). This section also monitors the flow rate (Q_D) hydrograph (no experimental time series are available at this section).

The origin of the numerical domain is located at the centre of the reservoir outlet section (at the floodplain height) and lies on the symmetry plane. Three sub-domains are detected: the water reservoir (triggering the flood), the very short discharge channel with the mobile gate, and the floodplain with the building matrix (Figure 4.1). The floodplain extends from the domain origin until x_{max}=3.00m and y_{max}=5.50m, as defined in Kim et al. (2015, [30]). The numerical domain only considers half physical domain (i.e. x≥0), taking advantage from a numerical vertical symmetry plane (x=0), which halves both the water reservoir and the discharge channel.

Further, the reservoir fluid below the floodplain height (z=0) is not simulated as it does neither leak from the reservoir nor appreciably influences the dynamics of the above fluid masses. The reservoir outlet section actually simulated is 0.500m-wide. The discharge channel is 0.250m-long. The initial volume of the water reservoir is $\omega_{res,0}=L_{res}\cdot W_{res}\cdot h_{res,0}$, with L_{res}=15.000m and W_{res}=5.000m.

The numerical model of Kim et al. (2015, [30]) represents the state-of-the-art code for this test case. It only simulates the floodplain and seems to provide no information about the boundary conditions at the reservoir outlet section. This issue does not affect this study as SPHERA simulates all the three subdomains.

Kim et al. (2015, [30]) approximate the dam break as an instantaneous event thus avoiding the direct representation of the mobile gate and its interactions with the fluid domain. This assumption was justified considering that the gate opening time (t_g=2.778s) were negligible with respect to the phenomenon duration. Here, the SPH results alternatively consider an instantaneous dam break and a progressive dam break with a mobile gate, more accurate, but computationally more expensive. The mobile gate is simulated as a rigid body with imposed kinematics and dimensions $L_{gx}\times L_{gy}\times L_{gz}$=0.500m×0.250m×0.500m, initial barycentre ($x_{g,0}$;$y_{g,0}$;$z_{g,0}$)=(0.250m;-0.125m;0.250m), velocity equal to either ($u_{g,0}$;$v_{g,0}$;$w_{g,0}$)=(0.180m/s;0.000m/s;0.000m/s), with time lower than t_g (when the mobile gate completes the opening), or the null vector, for later times.

The SPH spatial resolution is dx=0.025m. The spatial resolution in the solid domain of the gate is dx_s=3dx/5. The SPH simulation assumes h/dx=1.3 and the Courant-Friedrichs-Lewy number *CFL* is 0.125.

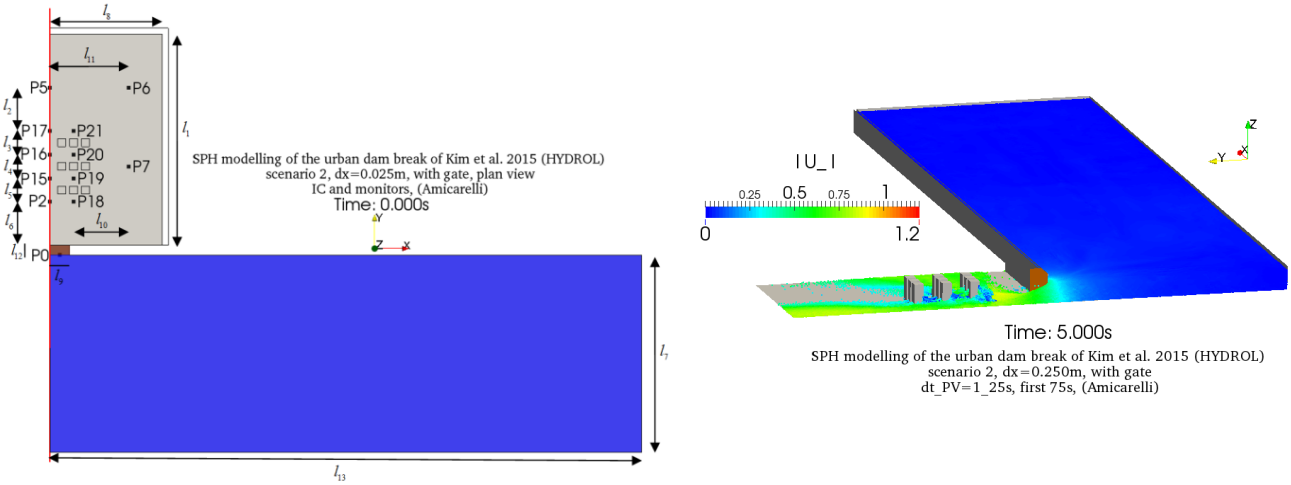

Figure 4.1. 3D urban dam-break flood (present SPH simulation of the experiment defined in Kim et al., 2015). Left panel. Initial conditions (top view; in the presence of the mobile gate -brown-; fluid domain -blue-), monitoring lines (black points) and symmetry plane (red). Numerical domain (half of the experimental domain). Lengths: l_1=5.350m, l_2=1.100m, l_3=0.600m, l_4=0.600m, l_5=0.600m, l_6=1.100m, l_7=5.000m, l_8=2.850m, l_9=0.500m, l_{10}=1.400m, l_{11}=2.000m, l_{12}=0.250m, l_{13}=15.000m. Right panel. Example of a 3D field (half domain) of the normalized velocity magnitude ("scenario 2") with a mobile gate (brown).

The validation of the SPH code is obtained by comparing the SPH hydrographs of the normalized water depth with the available measures (reported in Kim et al., 2015, [30]). A model inter-comparison is carried out by comparing the SPH hydrographs of velocity (averaged along the vertical) with the numerical results of the 2D porous Shallow Water Equations - Finite Volume Method (SWE-FVM) model of Kim et al. (2015, [30]). This porous 2D SWE-FVM model represents the "state-of-the-art" code for this test case and presents, with respect to SPHERA, some limits: Shallow-Water approximations (e.g., assumptions of pressure hydrostatic profiles and uniform velocity along the vertical); no direct resolution of the balance equations within the street canyons (building matrices); no modelling of the water reservoir; lack of information on the boundary conditions imposed at the reservoir outlet section.

Velocity vector, water depth, pressure, flow rate and reservoir volume (ω_{res}) are expressed in terms of non-dimensional quantities (U, H, T, the pressure coefficient Cp, Q and V_{res}, respectively):

$$\underline{U} \equiv \frac{\underline{u}}{\sqrt{2gh_{res,0}}}, \qquad H \equiv \frac{h}{h_{res}|_{t=0}}, \qquad T \equiv t\sqrt{\frac{h_{res}|_{t=0}}{2g}}, \qquad C_p \equiv \frac{p}{\rho g h_{res}|_{t=0}}$$
$$Q \equiv \frac{Q_D}{A_{out,\max}\sqrt{2gh_{res}|_{t=0}}} = \frac{Q_D}{b_{out}h_{res,0}\sqrt{2gh_{res}|_{t=0}}}, \qquad V_{res} \equiv \frac{\omega_{res}}{\omega_{res}|_{t=0}} \tag{4.1}$$

where $A_{out,max}$ and b_{out} are the maximum wet area and the width of the reservoir outlet section, respectively.

$(x_{B1};y_{B1})$=(0.300m;1.400m)	$(x_{B2};y_{B2})$=(0.600m;1.400m)	$(x_{B3};y_{B3})$=(0.900m;1.400m)
$(x_{B4};y_{B4})$=(0.300m;2.000m)	$(x_{B5};y_{B5})$=(0.600m;2.000m)	$(x_{B6};y_{B6})$=(0.900m;2.000m)
$(x_{B7};y_{B7})$=(0.300m;2.600m)	$(x_{B8};y_{B8})$=(0.600m;2.600m)	$(x_{B9};y_{B9})$=(0.900m;2.600m)

Table 4.1. Horizontal coordinates of the building barycentres (x≥0m).

$(x_{P2};y_{P2})$=(0.000m;1.100m)	$(x_{P5};y_{P5})$=(0.000m;4.000m)	$(x_{P6};y_{P6})$=(2.000m;4.000m)
$(x_{P7};y_{P7})$=(2.000m;2.000m)	$(x_{P15};y_{15})$=(0.000m;1.700m)	$(x_{P16};y_{P16})$=(0.00m;2.300m)
$(x_{P17};y_{P17})$=(0.000m;2.900m)	$(x_{P18};y_{P18})$=(0.600m;1.100m)	$(x_{P19};y_{P19})$=(0.600m;1.700m)
$(x_{P20};y_{P20})$=(0.600m;2.300m)	$(x_{P21};y_{P21})$=(0.600m;2.900m)	$(x_{P0};y_{P0})$=(0.250m;-0.250m)

Table 4.2. Horizontal coordinates of the monitoring lines (x≥0m).

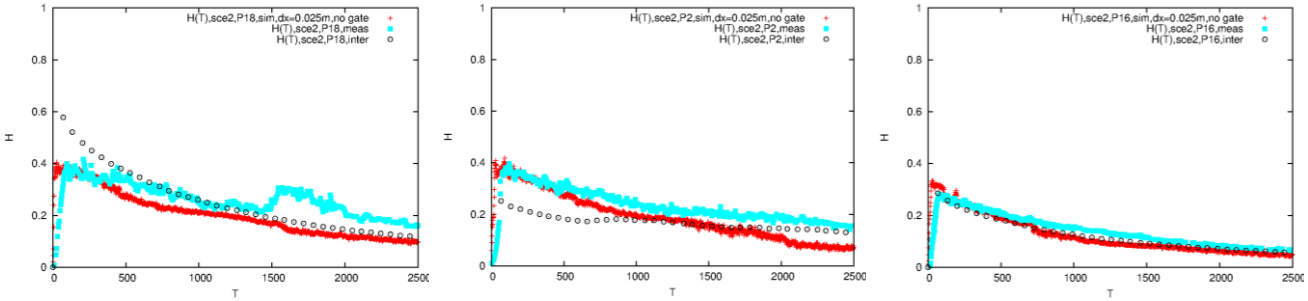

Figure 4.2. 3D urban dam-break flood (present SPH simulation of the experiment defined in Kim et al., 2015). Hydrographs of the non-dimensional water depth ("scenario 2"); validations and inter-comparisons; legend: + present SPH simulation, *dx*=0.025m, no gate; ■ measures (reported on Kim et al., 2015); ○ numerical results of the 2D SWE-FVM porous model (Kim et al., 2015).

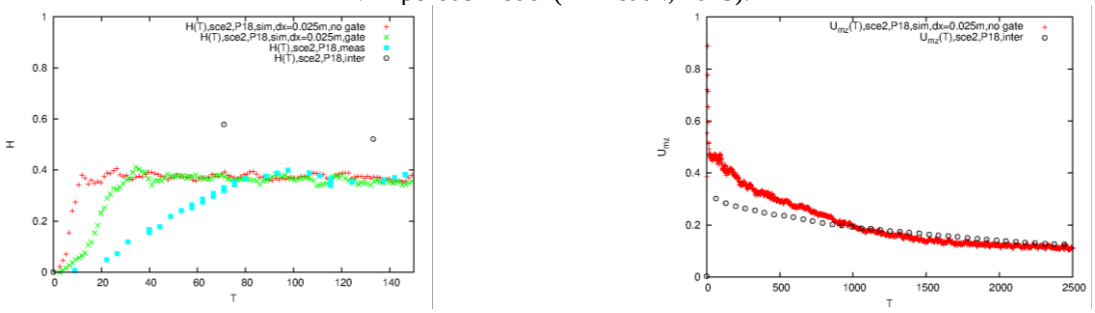

Figure 4.3. 3D urban dam-break flood (present SPH simulation of the experiment defined in Kim et al., 2015). Left panel. Hydrographs of the non-dimensional water depth ("scenario 2"); validations and inter-comparisons; Initial flood stage. Influence of the mobile gate. Right panel: Hydrographs of the normalized velocity magnitude ("scenario 2"); inter-comparisons. Legend: + present SPH simulation, *dx*=0.025m, no gate; × present SPH simulation, *dx*=0.025m, with gate; ■ measures (reported on Kim et al., 2015); ○ numerical results of the 2D SWE-FVM porous model (Kim et al., 2015).

The validation of the SPH code shows a correct representation of both the scenarios of this 3D urban flood, with better performance on the second scenario, featured by a more violent flood (Figure 4.2). During the flood regressive stage, the performance of the SPH code is comparable with the state-of-the-art code (Kim et al., 2015, [30]). During the most risky/intense flood stage (included the occurrence of the water depth peaks), the SPH code seems to provide more accurate results than the state-of-the-art code (Figure 4.2).

The direct representation of the mobile gate allows reducing the errors during the initial flood stage (Figure 4.3).

Velocity hydrograph inter-comparisons are influenced by the different model behaviour in the representation of the water depth hydrograph. For example, the hydrograph in Figure 4.3 shows an appreciable difference between the SPH model and the SWE-FVM model only during the most risky flood stage (T<1000), where the SPH model provides numerical results closer to the measured values (Figure 4.2).

With the aim of testing the numerical scheme for sediment transport (Amicarelli et al., 2017, [5]), a variant of previous test case has been considered with a non-cohesive sediment deposit (solid phase density ρ_s=2650kg/m^3; effective porosity ε_f=0.35; internal friction angle φ=38°; median diameter d_{50}=1.0mm) placed just downstream the gate (Figure 4.4). In this case the viscous criterion for numerical stability dominates, thus lowering significantly the time step duration before the granular material has been completely flushed by the water. In order to maintain the computational time to a suitable level, limiting viscosity has been activated (Manenti et al., 2018, [35]). Figure 4.4 shows in the left-hand panel the initial configuration with the sediment deposit (red colour); the density field has been normalized with respect to water density. The right-hand panel shows the normalized velocity field at 2.5s; besides reducing the position of the leading edge along the symmetry plane, the sediment deposit induces an upstream recirculation of the incoming water toward the wall of the

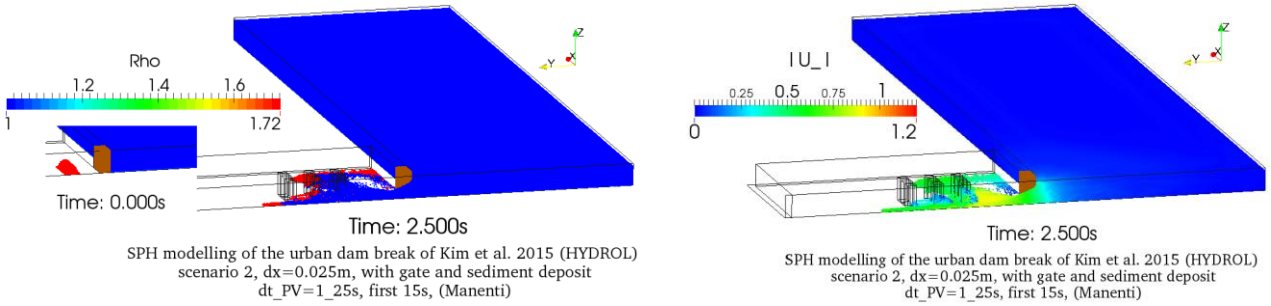

Figure 4.4. Variant of 3D urban dam-break flood with sediment deposit downstream the gate. Left panel: media (mobile gate -brown-; fluid domain -blue-; sediment deposit -red-; perspective view). Right panel: example of a 3D field of the normalized velocity magnitude ("scenario 2") with mobile gate (brown) and sediment deposit.

reservoir. After five seconds, the sediment particles are almost completely flushed away and subsequent evolution of the flow field is identical to the analogous simulation without the sediment deposit shown in Fig. 4.1.

5. 3D DAM-BREAK FLOOD WITH FULL-SCALE REAL TOPOGRAPHY, RESIDENTIAL AREAS AND ELECTRICAL SUBSTATIONS

SPHERA is applied to a 3D demonstrative and innovative test case, the Alpe Gera dam-break flood, which interacts with the lower hydroelectric reservoir of Campo Moro and propagates over the residential areas of Lanzada's municipality (Lanzada, Franscia, Tornadri e Ganda; Sondrio, Italy), causing the flooding of two electrical substations of Lanzada (with assessment of the associated damage). Some innovative features are highlighted: the representation of a dam-break flood by means of a 3D SPH-CFD code on full-scale real topography (ad-hoc elaboration of the raw Digital Elevation Model of SRTM3/DTED1 -USGS, [52]-), as a possible catastrophe triggered by an accident in a major power plant; the 3D CFD-SPH simulation of a flood propagating over several residential areas; the application of the substation-flooding damage model on a real and complex test case, with the simultaneous representation of several electrical substations.

Alpe Gera dam is the highest Italian operating dam (crown height of 160m) and the 13th in terms of reservoir volume (68.1Mm^3; ENEL, 2017, [17]; ITCOLD, [28]; INGAM, [27]). This gravity dam for hydroelectric use was built in 1962 (Valmalenco, province of Sondrio, Lombardia region, Italy). The dam-break is represented by an instantaneous and (almost) complete dam break of Alpe Gera, as a worst-case scenario with 500-year return period (according to the Italian laws), whereas the downstream dam of Campo Moro has no failure during the whole event. The whole dam-break flood propagation is simulated in terms of 3D CFD modelling and no analytical approximation is assumed either to represent the dam-break flow rate or to simplify the problem. The 3D dam structure is uninfluential for the selected dam-break scenario, is shown on Google Earth or analogous web sites (9.9446°E, 46.3146°N) and has been removed almost completely from the DEM used for this test case. The domain dimension is 7.9km×9.9km. The origin of the reference system is 9.0000°E, 46.0000°N. The terrain slope downstream the reservoir system is ca.16% and no appreciable river or stream reach is crossed by the numerical domain. Table 5.1 synthesizes the dam scalar quantities.

Dam quantity	Alpe Gera concrete dam	Campo Moro concrete dam
Geographic coordinates of the dam barycentre (°)	9.9446°E, 46.3146°N	9.9272°E, 46.3055°N
Cartesian coordinates of the dam barycentre (m)	x_1=72600m, y_1=35122m	x_2=71325m, y_2=33955m
Reservoir level (m)	2'125	1'953
Crown level (m)	2'128	1'954
Dam height (m)	160	20
Reservoir characteristic length (10^3m)	1.3	1.1
Dam crest length (m)	527	464
Reservoir volume (10^6m3)	68.1	10.6
Maximum distance downstream the dam (10^3m)	9.7	8.0

Table 5.1. 3D SPH modelling of flood propagation on residential areas and substation-flooding damage. Demonstrative test case: Alpe Gera dam-break flood, residential areas and electrical substations of Lanzada (Sondrio, Italy). Dam scalar quantities.

The large, but limited volumes of the hydroelectric reservoirs of the present demonstrative test case did not request a multi-resolution approach, which might be mandatory in other applications (e.g., Vacondio et al., 2012, [54]). Nonetheless, SPHERA could take advantage from improving its HPC features to reach finer spatial resolutions and higher numbers of SPH particles per simulation.

The 3D liquid domain configuration of this flood is complex. At the edges of the liquid domain, the following features are detected: wave breakings; dry enclaves of the liquid domain; multiple branches of the water front; stagnation zones; wet areas interested by high intermittency; run-up phenomena; highly non-stationary regime characterized by inertial gravity-driven flows (e.g., the Southern slope of Lanzada's valley is more affected by the flood than the Northern slope); water front atomization effects; temporary formation of a waterfall. An alternative representation by

means of 1D (or best 2D) Finite Difference (or best Finite Volume) codes, more commonly used, could be only carried out in a much more simplified way, with respect to the SPH code.
All the 4 simulated residential areas are struck by the violent flood. After a preliminary stage characterized by water front atomization effects, the territory of the hamlet of Franscia is most flooded in the period 105s<t<660s, whereas the compact flood front reaches the residential areas of Tornadri, Ganda e Lanzada at t=ca.125s, t=ca.140s and t=ca.152s, respectively.
Starting from its estimation of the 3D non-stationary fluid dynamics fields, SPHERA also produces the 2D synthetic fields (Figure 5.3.) of the maximum water depth and the maximum specific (per width unit) flow rate. These variables are useful to assess the flood-related damage, in a more accurate and complex way than the most common damage models, which obtain flood-related data as scalar values (0D), 1D fields, or by means of simplified empirical relationships.
The maximum water depth (Y_{max}, m) at the residential areas varies between several meters to several tenths of meters. The maximum specific flow rate q_{max}=ca.15.7×10^{3}m^2/s is simulated in the area interested by the two following jumps (associated to sudden section shrinkages) at the entrance of Lanzada's valley. Other relative maxima are located: at the outlet section of Alpe Gera dam; downstream the rocky spur close to Campo Moro dam; between the two reservoirs.
The hydrographs (Figure 5.4.) at the outlet sections of Alpe Gera (subscript "$_1$") and Campo Moro (subscript "$_2$") dams show that the maximum flow rates are $Q_{1,max}$=ca.387×10^{3}m^3/s and $Q_{2,max}$=ca.211×10^{3}m^3/s (peak time: t_p=86s), respectively. The flow rate at Campo Moro outlet section drops below 5% of Q_1,max since t=753s. The atomization phenomena affects "substation 1" since t=ca.101s, whereas the compact liquid front reaches this substation at t=ca.155s; the flow rate peak $Q_{s1,max}$=ca.244×10^{3}m^3/s is recorded at t_p=222s (the time fluctuations make this hydrograph irregular with several relative maxima). Thus, the red curve of Figure 5.4. represents the simulated dam-break flow rate at the outlet section of Alpe Gera dam.
The hydrographs of the water depth at the outlet section of Campo Moro tends to the final value of Y_2=ca.25m, 5-meter higher than the initial water depth. The hydrograph of the water depth for "substation 1" shows much lower values and is characterized by a large wet edge and high intermittency all over the phenomenon duration.

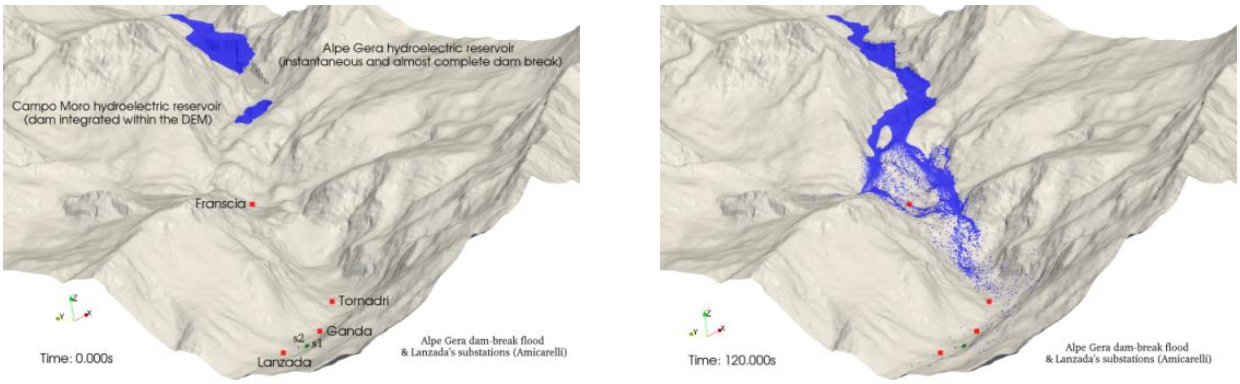

Figure 5.1. 3D SPH modelling of flood propagation on residential areas and substation-flooding damage. Demonstrative test case: Alpe Gera dam-break flood, residential areas and electrical substations of Lanzada. Examples of 3D views and target identification: fluid domain (blue), DEM (grey), residential areas of the municipality of Lanzada (each one is indicated by a red square located within the associate area), "substation 1" ("*s1*", green), "substation 2" ("*s2*", black). Municipality of Lanzada (province of Sondrio; region Lombardia; Italy); latitude ca.46°18'52"N, longitude ca.9°56'40"E. 3D situation plan (left panel) and SPH simulation at t=120s (right panel).

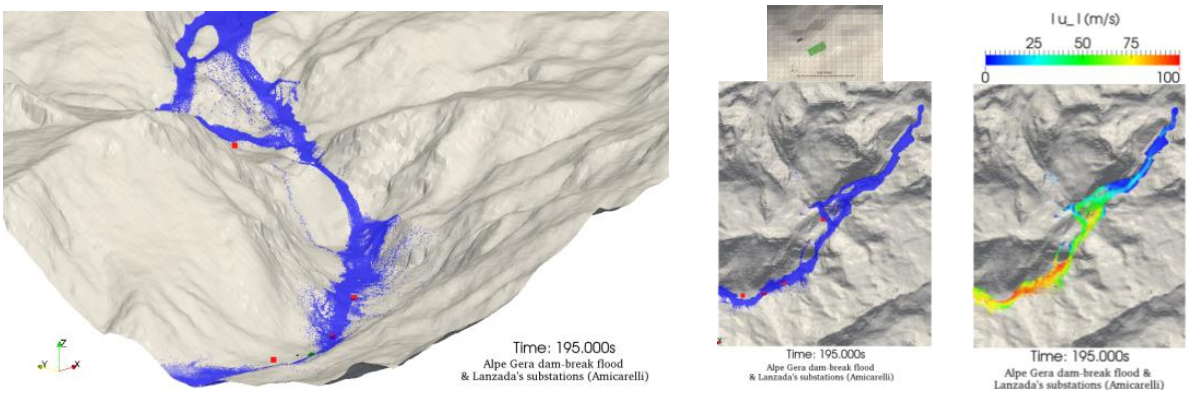

Figure 5.2. 3D SPH modelling of flood propagation on residential areas and substation-flooding damage. Demonstrative test case: Alpe Gera dam-break flood, residential areas and electrical substations of Lanzada (Sondrio, Italy). Example of the spatial evolution of the liquid domain at a fixed time and identification of the flood targets (residential areas and electrical substations): detail of a 3D view (downstream sub-domain; left panel); plan view (bottom centre panel). Detail of the DEM (with brown vertices) around "substation 1" (transparent green) and "substation 2" (transparent black; top centre panel). Example of the field of the velocity magnitude (plan view, right panel).

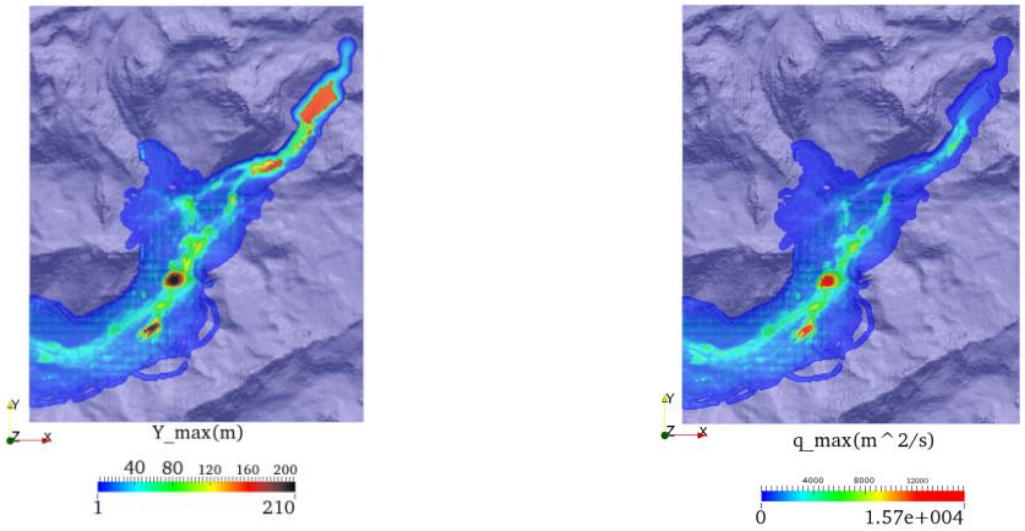

Figure 5.3. 3D SPH modelling of flood propagation on residential areas and substation-flooding damage. Demonstrative test case: Alpe Gera dam-break flood, residential areas and electrical substations of Lanzada (Sondrio, Italy). 2D synthetic fields of the maximum water depth (left panel) and the maximum specific flow rate (right panel).

Even without additional actions (e.g., rising of the crown height), Campo Moro dam partially behaves as a flood-control dam. At the end of the simulation, the volume leaked from Alpe Gera reservoir has been partially (12%) stored within Campo Moro reservoir and has mainly (88%)

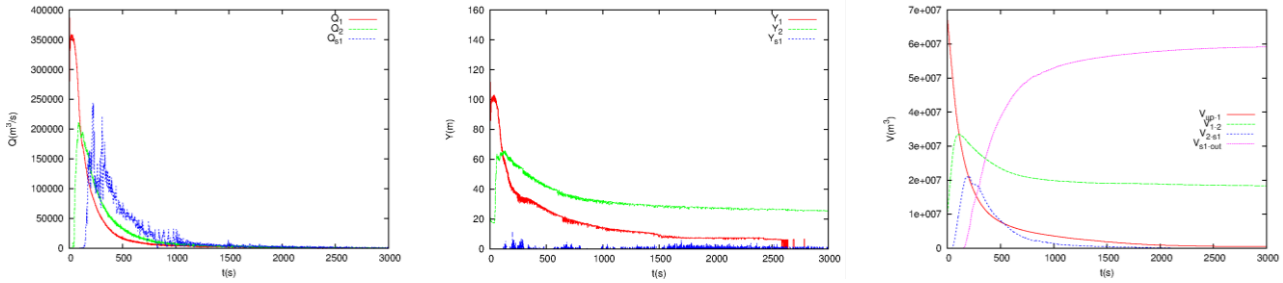

Figure 5.4. 3D SPH modelling of flood propagation on residential areas and substation-flooding damage. Demonstrative test case: Alpe Gera dam-break flood, residential areas and electrical substations of Lanzada (Sondrio, Italy). Hydrographs of the flow rate (left panel) and the water depth (centre panel) at the outlet sections of Alpe Gera ("$_1$") and Campo Moro ("$_2$") reservoirs, and at the section passing for the "substation 1" ("$_{s1}$"). Hydrographs of the water volumes (right panel) cumulated upstream the outlet section of Alpe Gera reservoir ("$_{up\text{-}1}$"), between the dams of Alpe Gera and Campo Moro ("$_{1\text{-}2}$"), between Campo Moro outlet section and the "substation 1" ("$_{2\text{-}s1}$") and downstream this substation ("$_{s1\text{-}out}$").

Distance from the main dam (10^3m)	Maximum flow rate (10^3m^3/s)	Flow-rate peak time (s)	Maximum water depth (m)	Water-depth peak time (s)
0.0 (Alpe Gera)	387	4	160	0
1.7 (Campo Moro)	211	86	65	90
7.5 (section barycentre: x_{s1}=67261m, y_{s1}=29825m)	244	222	18	199

Table 5.2. 3D SPH modelling of flood propagation on residential areas and substation-flooding damage. Demonstrative test case: Alpe Gera dam-break flood, residential areas and electrical substations of Lanzada (Sondrio, Italy). Maximum flow rate and water depth, and associated peak times. The water depths refer to the section barycentre. The last monitoring section contains the barycentre of the substation 1 (the section barycentre is different from the substation barycentre).

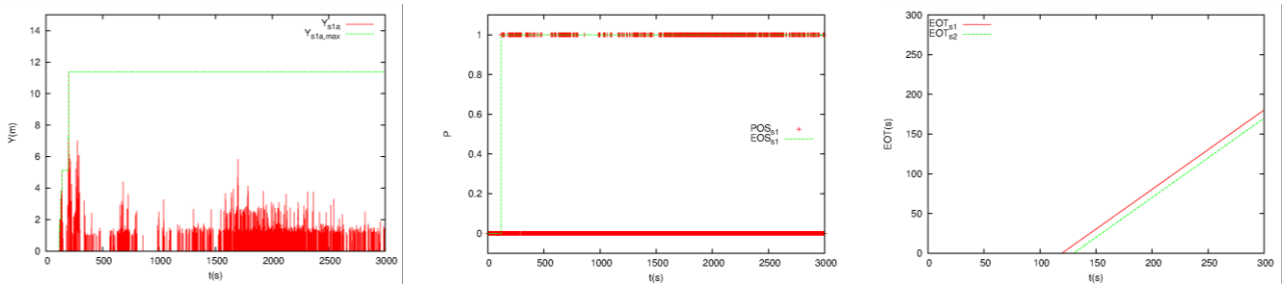

Figure 5.5. 3D SPH modelling of flood propagation on residential areas and substation-flooding damage. Demonstrative test case: Alpe Gera dam-break flood, residential areas and electrical substations of Lanzada (Sondrio, Italy). Vulnerability and "proxy" damage on blackouts triggered by electrical substation flooding, with no redundancy of the electric grid (substation 1, "$_{s1}$"; substation 2, "$_{s2}$"). Time series: substation water depth ("Y_{sub}" or "Y_s") and update of its maximum value during the flood event ("$Y_{sub,max}$" o "$Y_{s,max}$"; left panel); Probability of a power Outage Start (*POS*), Expected power Outage Status (*EOS*; centre panel); update of the Estimated Outage Time/duration (*EOT*; right panel).

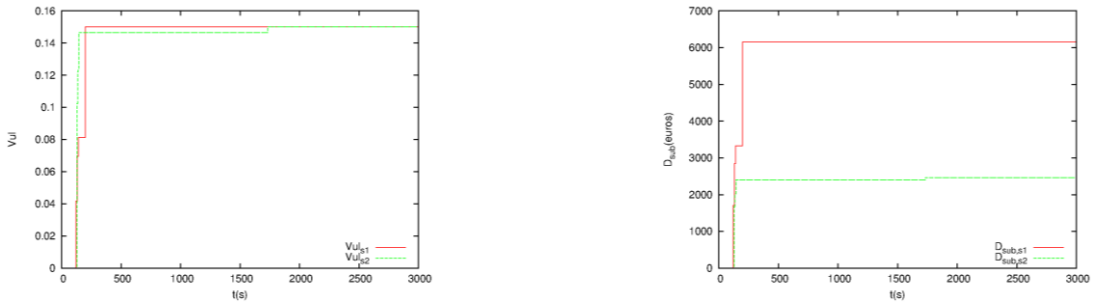

Figure 5.6. 3D SPH modelling of flood propagation on residential areas and substation-flooding damage. Demonstrative test case: Alpe Gera dam-break flood, residential areas and electrical substations of Lanzada (Sondrio, Italy). Time series of the substation-flooding vulnerability (left panel) and damage (right panel) limited to the components of the electrical substations.

crossed the domain and flown downstream the municipality of Lanzada (Alpe Gera residual reservoir volume is 1% of its initial value; the dam break is almost complete and the bathymetry is unavailable, but numerically elaborated).

Table 5.2 synthesizes some scalar SPH output data, already discussed in the previous figures. The maximum water depth and flow rate almost occur simultaneously (within 4s), at a given dam. A relevant decrease features both the water depth and the flow rate moving from the main dam to the minor dam (1.7km downstream). At the monitoring section containing the "substation 1", the peak time for the flow rate occurs 23s after the peak time for the water depth. Here both the variables show very irregular up to intermittent time evolutions and the peak values are only reached instantaneously.

In terms of power-outage damage (Figure 5.5.), as the flood is extremely violent, the possible presence of an appreciable water depth on the substation areas almost always coincides with the triggering of a blackout event (*POS*=1). The intermittency factor of *POS* at the "substation 1" (γ_{s1}=0.881) shows that in the 11.9% of the monitored period a blackout event would be triggered at

this substation (in case an outage were not yet present), under the hypothesis of no redundancy of the power grid. The *POS* intermittency factor for the "substation 2" (γ_{s2}=0.983) indicates that in the 1.7% of the simulated period a blackout event would be triggered at this substation, under the same hypothesis above. Both "substation 1" and "substation 2" are interested by prolonged blackout events starting from t=120s and t=130s, respectively (ref., time series of *EOS* and *EOT*). As the restoration times of the electrical infrastructures are much higher than the time scale of this flood, once the first blackout event is triggered, the outage lasts until the end of the simulation. For this application, *EOT* is then ruled by the restoration time, which is assumed equal to 11 hours (Sec.3.1.1), as a worst-case estimation (this flood is catastrophic) and in the absence of more accurate input data.

In terms of damage limited to the components of the electrical substations (Figure 5.6.), the time series of the flood-induced vulnerability show that since t=1'732s both the substations have been submerged with water depths higher than 10m, causing the maximum flood-related vulnerability of the substations (15%, $V_{u,sub}$=0.15). They are affected by different damage, as function of their type and value. The substation-flooding damage for the components of the high-voltage "substation 1" and the medium-voltage "substation 2" are $D_{sub,s1}$=6'150euros and $D_{sub,s2}$=2'460euros, respectively.

The results of the demonstrative test case have actually permitted to achieve several targets at the same time: the representation of a dam-break flood by means of a 3D SPH-CFD code on complex topography, as a possible catastrophe triggered by an accident in a major power plant; the 3D CFD-SPH simulation of a flood propagating over several residential areas, even though the spatial resolution of the free DEM did not permit an explicit modelling of the buildings and the urban canyons; the application of the substation-flooding damage model on a real and complex test case, with the simultaneous representation of several electrical substations. Considering the very different demonstrative targets simultaneously achieved by within the same test case, it is not surprising that, for this catastrophic flood, the flood-related damage limited to the components of the electrical substations are negligible with respect to the number of possible fatalities and the overall damage (which also provides for the blackout events).

6. CONCLUSIONS

The Smoothed Particle Hydrodynamics code SPHERA (RSE SpA) has been validated on two scenarios of a laboratory urban dam-break flood. Validations refer to the predicted water depth. Model inter-comparisons on velocity and water depth involve the numerical results of a state-of-the-art code, based on a porous Shallow Water Equations - Finite Volume Method 2D model. SPHERA provides a performance comparable with the state-of-the-art code, with results closer to the measured values during the most risky flood stage, especially in terms of water depth maxima. Both codes provided a satisfactorily representation of water depth and also share the same limits (e.g., omission of the delayed water level rise at one monitoring line). One might consider that both 2D and 3D CFD codes for flood propagation have been rarely compared with measures in the presence of an urban canopy. During the first stages of flood propagation, further improvements of SPHERA results have been achieved by a direct modelling of the mobile gate causing the dam-break flood. Herein SPHERA has also been empowered with a substation-flooding damage model. The model distinguishes the functional damage due to out of service periods from the material damage to the components of the electrical substations. SPHERA has finally been applied to a full-scale catastrophic 3D dam-break flood, which propagates on real topography, interacts with a lower hydroelectric reservoir, covers four residential areas and two electrical substations, whose related damage is assessed.

With respect to the state-of-the-art model, the SPH code shows several advantages: better representation of the most risky/intense flood stage (included the water depth maxima); simulation of the reservoir with neither simplifications nor calibrations (ref., outlet section of the reservoir); simulation of a progressive dam break (beyond the more approximated instantaneous dam break) by means of explicit simulation of the mobile gate, to improve the representation of the flood initial stage; use of a numerical symmetry plane (boundary conditions) to only simulate half domain taking advantage from the experimental symmetry conditions; possible simulation of transported solid structures (e.g., vehicles, tree trunks) and granular material; 3D modelling (the state-of-the-art porous model is 2D, with Shallow-Water approximation: hydrostatic pressure profiles, velocity is uniform along the vertical, …); detailed fluid dynamics analysis within the urban canopy (urban fabric), included fluid-structure interactions (the porous models do not provide a direct modelling of the flood-building interactions); effective performance even at coarse spatial resolution (for preliminary analyses).

SPHERA has revealed suitable to the substation-flooding risk analyses as it is featured by: 3D CFD-SPH modelling of floods (and fast landslides) also in residential areas; estimation of the synthetic 2D fields of the maximum water depth and the maximum specific flow rate (derived from the non-stationary 3D fluid dynamics fields); simulation of the time series of resulting force and torque, and the maximum pressure over solid structures; use of any DEM, with possible and approximated reconstruction of the bathymetry (in case it is unavailable); design of actions/works and scenario simulations, also by modifying the DEM with digging and filling areas; 3D transport of solid structures and their interactions with other mobile and fixed structures; 3D bed-load transport and its impact on mobile and fixed solid structures; simulation of flood-control works (e.g., flood-control dam); simulation of surface waves within water reservoirs; applicability to any complex site with a domain cover up to some hundreds of squared kilometres; model for vulnerability and "proxy" damage due to substation-flooding blackouts, in the absence of power grid redundancy (at the level of the single substations) and possibility of coupling with a power grid model for a more accurate damage model; complete assessment of the substation-flooding damage on the components of the electrical substations; free use and reproducibility of the test cases (SPHERA is FOSS); direct estimation of the position of the free surface and the fluid and phase interfaces; direct representation of Lagrangian derivatives (absence of advective non-linear term at the Left Hand Side of the balance equations); "mesh-less" method; no iterative algorithms to solve the main balance equations (Weakly Compressible Approach - SPH). At the same time, SPH is slightly more time consuming then mesh-based methods (for accurate simulations, fixed the same

spatial resolution) and has a narrower but peculiar range of application fields, whose number is nonetheless elevated and involve floods.
SPHERA has been applied to the following application fields: floods with transport of solid bodies and bed-load transport; fast landslides and their interactions with water reservoirs; sediment removal from water bodies; fuel sloshing tanks. SPHERA is developed and distributed on a GitHub public repository (SPHERA, 2019, [49]) with more than thirty tutorials (included the input files associated to this study), thus allowing the code availability and possible modification, and the repeatability of the published test cases. The whole numerical chain of SPHERA is free. SPHERA indexed by the SPH International Community SPHERIC (2019, [50]).

Acknowledgements.
This study has been financed by the Research Fund for the Italian Electrical System (for "Ricerca di Sistema -RdS-"), at different stages:

- ✓ under the Contract Agreement between RSE SpA and the Italian Ministry of Economic Development for the RdS period 2015-2017, in compliance with the Decree of 21 April 2016. Reference project: 'A.5 - Sicurezza e vulnerabilità del sistema elettrico', Frigerio A. et al., 2015-2018
- ✓ in compliance with the Decree of Minister of Economic Development April 16, 2018

except for the contributions provided by University of Pavia (simulation of Fig.4.4) and IMT School for Advanced Studies Lucca (paper supervision).
"We acknowledge the CINECA award under the ISCRA initiative, for the availability of High Performance Computing resources and support." In fact, SPHERA simulations of this study has been financed by means of the following instrumental funding HPC projects: HSPHCS9, HSPHERA9, HPCEFM18, FLR-RMPV, TNMRA01, HPCEFM7b, HPCEFM17, NMTFEPRA, HPCNHLW1.
SPHERA v.9.0.0 (RSE SpA) is realised thanks to the funding "Fondo di Ricerca per il Sistema Elettrico" within the frame of a Program Agreement between RSE SpA and the Italian Ministry of Economic Development (Ministero dello Sviluppo Economico).

The release of the FOSS versions of SPHERA has been supported in RSE and promoted by the Department Director Michele de Nigris, the Deputy Director and Project Manager Antonella Frigerio, the Project Manager Francesco Apadula (since 2020) and the Research Team Managers Guido Pirovano (since 2016) and Massimo Meghella (during the period 2015-2016).
The raw DEM for the Alpe Gera dam break scenarios is released by SRTM3/DTED1 (USGS).

References.

1. Abdelrazek A.M., I. Kimura, Y. Shimizu; 2016; Simulation of three-dimensional rapid free-surface granular flow past different types of obstructions using the SPH method; Journal of Glaciology, 62(232):335-347.
2. Adami S., X.Y. Hu, N.A. Adams; 2012; A generalized wall boundary condition for smoothed particle hydrodynamics; Journal of Computational Physics, 231:7057–7075.
3. Amicarelli A., G. Agate, R. Guandalini; 2013; A 3D Fully Lagrangian Smoothed Particle Hydrodynamics model with both volume and surface discrete elements; International Journal for Numerical Methods in Engineering, 95: 419–450, DOI: 10.1002/nme.4514.
4. Amicarelli A., R. Albano, D. Mirauda, G. Agate, A. Sole, R. Guandalini; 2015; A Smoothed Particle Hydrodynamics model for 3D solid body transport in free surface flows; Computers & Fluids, 116:205–228. DOI 10.1016/j.compfluid.2015.04.018
5. Amicarelli A., B. Kocak, S. Sibilla, J. Grabe; 2017; A 3D Smoothed Particle Hydrodynamics model for erosional dam-break floods; International Journal of Computational Fluid Dynamics, 31(10):413-434; DOI 10.1080/10618562.2017.1422731
6. Amicarelli A., S. Manenti, R. Albano, G. Agate, M. Paggi, L. Longoni, D. Mirauda, L. Ziane, G. Viccione, S. Todeschini, A. Sole, L.M. Baldini, D. Brambilla, M. Papini, M.C. Khellaf, B. Tagliafierro, L. Sarno, G. Pirovano; 2020; SPHERA v.9.0.0: a Computational Fluid Dynamics research code, based on the Smoothed Particle Hydrodynamics mesh-less method; Computer Physics Communications, 250:107157; https://doi.org/10.1016/j.cpc.2020.107157
7. Bui Ha H., R. Fukagawa, K. Sako, S. Ohno; 2008; Lagrangian meshfree particles method (SPH) for large deformation and failure flows of geomaterial using elastic–plastic soil constitutive model; Int. J. Numer. Anal. Meth. Geomech., 32:1537-1570.
8. Cea L., M.E. Vázquez-Cendón; 2010; Unstructured finite volume discretization of two-dimensional depth-averaged shallow water equations with porosity; Int. J. Num. Meth. Fluid, 63:903-930.
9. Chen A., B. Evans, S. Djordjevic, D.A. Savic; 2012; A coarse-grid approach to represent building blockage effects in 2D urban flood modelling; J. Hydrol., 426-427:1-16.
10. Chow M., L. Taylor, M. Chow; 1996; Time of outage restoration analysis in distribution systems; IEEE Transactions on Power Delivery. 11(3):1652-1658.
11. Colagrossi A., A. Souto-Iglesias, M. Antuono, S. Marrone; 2013; Smoothed-particle-hydrodynamics modeling of dissipation mechanisms in gravity waves; Physical Review E - Statistical, Nonlinear, and Soft Matter Physics, 87(2), art. no. 023302.
12. Crawford M., S. Seidel; 2013; Weathering the storm: building business resilience to climate change. Center for climate and energy solutions: Arlington, VA.
13. Danis M.E., M. Orhan, A. Ecder; 2013; ISPH modelling of transient natural convection; International Journal of Computational Fluid Dynamics, 27(1):15-31.
14. Di Monaco A., S. Manenti, M. Gallati, S. Sibilla, G. Agate, R. Guandalini; 2011; SPH modeling of solid boundaries through a semi-analytic approach. Engineering Applications of Computational Fluid Mechanics, 5(1):1-15.
15. Electricity North West Limited; 2017; Electricity Policy Document 355, Issue 3 April 2017, Substation Flood Protection.
16. EM-DAT; 2012; EM-DAT: Disasters in numbers (October 2000), International Disaster Database, Université catholique de Louvain Brussels, Belgium; www.emdat.be (last access: 11 February 2019)
17. ENEL (Unità di Business Idroelettrica di Sondrio); 2017; Sistema idroelettrico della VALMALENCO; La Diga di ALPE GERA.
18. Ferrand M., D.R. Laurence, B.D. Rogers, D. Violeau, C. Kassiotis; 2013; Unified semi-analytical wall boundary conditions for inviscid laminar or turbulent flows in the meshless SPH method: International Journal for Numerical Methods in Fluids, 71(4):446-472.

19. Gomez-Gesteira M., B.D. Rogers, R.A. Dalrymple, A.J.C. Crespo; 2010; State-of-the-art of classical SPH for free-surface flows; Journal of Hydraulic Research, 48(Extra Issue):6-27; doi:10.3826/jhr.2010.0012
20. Gu S., X. Zheng, L. Ren, H. Xie, Y. Huang, J. Wei, S. Shao; 2017; SWE-SPHysics simulation of dam break flows at South-Gate Gorges Reservoir; Water (Switzerland), 9(6), art. no. 387.
21. Guinot V.; 2012; Multiple porosity shallow water models for macroscopic modelling of urban floods; Adv. Water Resour., 37:40-72.
22. Guo, K., Sun, P.N., Cao, X.Y. and Huang, X., 2017. A 3-D SPH model for simulating water flooding of a damaged floating structure. Journal of Hydrodynamics, Ser. B, 29(5), pp.831-844.
23. Hashemi M.R., R. Fatehi, M.T. Manzari; 2012; A modified SPH method for simulating motion of rigid bodies in Newtonian fluid flows; International Journal of Non-Linear Mechanics, 47:626–638.
24. Hazus-MH; 2011; Technical Manual, Multi-hazard Loss Estimation Methodology, Flood Model; Department of Homeland Security, Federal Emergency Management Agency, Mitigation Division, Washington, D.C.
25. He J., N. Tofighi, M. Yildiz, J. Lei, A. Suleman A.; 2017; A coupled WC-TL SPH method for simulation of hydroelastic problems; International Journal of Computational Fluid Dynamics, 31(3):174-187.
26. Holmes M.; 2015; Water infrastructure vulnerability due to dependency on third party infrastructure sectors; School of Civil Engineering and Geosciences, Newcastle University, May 2015; Doctorate thesis.
27. INGAM, http://www.ingam.com/dighe/elenco-dighe.html (last access on 14 June2019)
28. ITCOLD, http://www.itcold.it/ (last access on 14 June2019)
29. Khayyer A., Gotoh H., Falahaty H., Shimizu Y.; 2018; An enhanced ISPH–SPH coupled method for simulation of incompressible fluid-elastic structure interactions; Computer Physics Communications, 232:139-164.
30. Kim B., B.F. Sanders, J.S. Famiglietti, V. Guinot; 2015; Urban flood modeling with porous shallow-water equations: A case study of model errors in the presence of anisotropic porosity; Journal of Hydrology, 523:680-692.
31. Le Touzé D., A. Colagrossi, G. Colicchio, M. Greco; 2013; A critical investigation of smoothed particle hydrodynamics applied to problems with free-surfaces; Int. J. Numer. Meth. Fluids, 73:660-691; DOI: 10.1002/fld.3819
32. Liang, Q., Xia, X. and Hou, J., 2015. Efficient urban flood simulation using a GPU-accelerated SPH model. Environmental Earth Sciences,74(11), pp.7285-7294.
33. Macia F., L.M. Gonzalez, J.L. Cercos-Pita; A. Souto-Iglesias; 2012; A Boundary Integral SPH Formulation - Consistency and Applications to ISPH and WCSPH-; Progress of Theoretical Physics, 128-3, 439-462.
34. Maliszewski P., C. Perrings; 2012; Factors in the resilience of electrical power distribution infrastructures; Applied Geography, 32:668-679.
35. Manenti S., Amicarelli A., Todeschini S; 2018; WCSPH with Limiting Viscosity for Modeling Landslide Hazard at the Slopes of Artificial Reservoir; Water, 10, 515. doi:10.3390/w10040515.
36. Manenti S.; D. Wang; J.M. Domínguez; D. Li; A. Amicarelli; R. Albano; 2019; SPH Modeling of Water-Related Natural Hazards; Water, 11(9):1-26; https://doi.org/10.3390/w11091875
37. Manenti S., S. Sibilla, M. Gallati, G. Agate, R. Guandalini; 2012; SPH Simulation of Sediment Flushing Induced by a Rapid Water Flow; Journal of Hydraulic Engineering ASCE 138(3):272-284.
38. Marongiu J.C.; F. Leboeuf, J. Caro, E. Parkinson; 2010; Free surface flows simulations in Pelton turbines using an hybrid SPH-ALE method; J. Hydraul. Res., 47:40–49.
39. Mayrhofer A, Rogers BD, Violeau D, Ferrand M.; 2013; Investigation of wall bounded flows using SPH and the uni fied semi-analytical wall boundary conditions. Computer Physics Communications 184, 2515–2527.

40. Ministero dell'Ambiente e della Tutela del Territorio e del Mare (MATTM); 2019; Infrastrutture elettriche presenti sul territorio italiano; http://sinva.ancitel.it/mapviewer/index.html?collection=http://sinva.ancitel.it/WMC/Collection/VA/D5DB339E-DB14-9144-B043-B141DCABC108&context=http://sinva.ancitel.it/WMC/Context/VA/D5DB339E-DB14-9144-B043-B141DCABC108/963AD4B4-906A-4E53-B7FC-F497C3997138&v=full (last access on 13 June 2019)
41. Monaghan JJ. Smoothed particle hydrodynamics; 2005; Rep. Prog. Phys., 68:1703–1759.
42. Munich RE; 2010; NATURAL CATASTROPHE YEAR IN REVIEW; January 10, 2011; https://www.munichre.com/site/mram/get/documents_E-1545588599/mram/assetpool.mr_america/PDFs/4_Events/munich_re_2010_natcat_review.pdf (last access on 14 June 2019)
43. Price, D.J.; 2012; Smoothed Particle Hydrodynamics and Magnetohydrodynamics; J. Comp. Phys., 231(3): 759-794.
44. Reed D.; 2008; Electric utility distribution analysis for extreme winds; Journal of wind engineering and industrial aerodynamics, 96(1):123-140.
45. Sanders B.F.; 2008; Integration of a shallow-water model with a local time step; J. Hydraul. Res. 46(8):466-475.
46. Sanders B.F., J.E. Schubert, H.A. Gallegos; 2008; Integral formulation of shallow water equations with anisotropic porosity for urban flood modelling; J. Hydrol., 362:19-38.
47. Schubert J.E., B.F. Sanders; 2012; Building treatments for urban flood inundation models and implications for predictive skill and modeling efficiency; Adv. Water Resour. 41:49-64.
48. Shadloo M.S., G. Oger, D. Le Touzé; 2016; Smoothed particle hydrodynamics method for fluid flows, towards industrial applications: Motivations, Current state, And challenges; Computers and Fluids, 136:11-34.
49. SPHERA v.9.0.0 (RSE SpA), https://github.com/AndreaAmicarelliRSE/SPHERA (last access on 11 November 2019)
50. SPHERIC (SPH scientific and industrial community affiliated to ERCOFTAC -European Research Community On Flow, Turbulence and Combustion-), http://spheric-sph.org/sph-projects-and-codes (last access on 14 June 2019)
51. Soares-Frazão S., J. Lhomme, V. Guinot, Y. Zech; 2008; Two-dimensional shallow water model with porosity for urban flood modelling; J. Hydraul. Res. 46(1):45-64.
52. SRTM3/DTED1 (USGS); http://earthexplorer.usgs.gov/ (last access on 13 June 2019)
53. Tsuruta N., Khayyer A., Gotoh H.; 2015; Space potential particles to enhance the stability of projection-based particle methods; International Journal of Computational Fluid Dynamics, 29(1):100-119; DOI: 10.1080/10618562.2015.1006130
54. Vacondio R, Rogers BD, Stansby P, Mignosa P.; 2012; SPH Modeling of Shallow Flow with Open Boundaries for Practical Flood Simulation; J. Hydraul. Eng., 138(6):530–541.
55. Vila J.P.; 1999; On particle weighted methods and Smooth Particle Hydrodynamics; Mathematical Models and Methods in Applied Sciences, 9(2):161-209.
56. Violeau D.; A. Leroy; 2014; On the maximum time step in weakly compressible SPH; Journal of Computational Physics, 256: 388-415.
57. Violeau D., B.D. Rogers; 2016; Smoothed particle hydrodynamics (SPH) for free-surface flows: past, present and future; Journal of Hydraulic Research, 54(1):1-26.
58. Wan H., Li R., Pu X., Zhang H., Feng J.; 2017; Numerical simulation for the air entrainment of aerated flow with an improved multiphase SPH model; International Journal of Computational Fluid Dynamics, 31(10):435-449; DOI: 10.1080/10618562.2017.1420175
59. Yu D., S.N. Lane; 2005; Urban fluvial flood modelling using a two dimensional diffusion-wave treatment, part 2: development of a sub-grid-scale treatment; Hydrol. Process. 20(7):1567-1583.